BMC Medical Genomics

RESEARCH

Open Access

Identification of an *F8* complex recombination in Chinese hemophilia a patient using long-read sequencing and optical genome mapping

Yuxin Zhang[1,2,3], Mingjie Yang[4], Lulu Yan[1,2,3], Chunxiao Han[1,2,3], Jiangyang Xue[1,2,3], Juan Geng[5], Changshui Chen[2], Lijun Bao[6], Bingqin Xu[6], Shanshan Wu[3,8*] and Haibo Li[1,2,3,7*]

Abstract

Background Hemophilia A (HA) is an X-linked recessive bleeding disorder caused by pathogenic variants in the *F8* gene, resulting in deficient coagulation factor VIII activity. Although intron 22 and intron 1 inversions (Inv22 and Inv1) accounts for approximately 50% of severe HA cases, complex structural rearrangements mediated by intron 22 homologous region (*int22h)* repeats have rarely reported and poorly characterized.

Methods In this study, we investigated a Chinese severe HA pedigree with a complex rearrangement of *F8* gene by integrating 750 K SNP arrays, long-read sequencing (Oxford Nanopore Technologies, ONT), and optical genome mapping (OGM). This multi-platform strategy enabled comprehensive characterization of the structural variations affecting the *F8* gene.

Results We identified a complex rearrangement in the proband's *F8* gene, characterized by sequential duplications inserted within intron 22. These include a 7.75 kb direct duplication involving a portion of *int22h-1*, a 78.78 kb inverted duplication containing partial sequences of *int22h-3* and *int22h-2*, and an 86.56 kb direct duplication spanning a portion of *int22h-3* and exons 2–8 of the *TMLHE* gene. The structural variation in the F8 gene of the proband was inherited from the mother.

Conclusion Our findings revealed that the complex rearrangement of *F8* is the genetic cause of HA in this pedigree. The combined use of OGM and ONT provides an effective approach for deciphering the characterization of complex structural variants and determining the orientation of inserted segments, although base-precision breakpoint mapping remains challenging in highly homologous regions.

Keywords *F8* gene, Hemophilia A, Optical genome map, Long-read sequencing, Complex structural variant

*Correspondence:
Shanshan Wu
wsszhuhe@163.com
Haibo Li
lihaibo-775@163.com

Full list of author information is available at the end of the article

Introduction

Hemophilia A (HA) is an X-linked recessive bleeding disorder caused by pathogenic variants in the *F8* gene encoding coagulation factor VIII [1]. It has a prevalence of approximately 1 in 5000 males worldwide. HA is clinically classified as severe (FVIII: C < 1%), moderate (1% ≤ FVIII: C < 5%), or mild (5% ≤ FVIII: C < 40%) on the basis of plasma FVIII activity (FVIII: C) [2]. The *F8* gene, located at the Xq28 locus on the distal long arm of the X chromosome, spans approximately 186 kb and comprises 26 exons interspersed with 25 introns [3]. Disruption of the *F8* gene caused by intron 22 inversion (Inv22) and intron 1 inversion (Inv1) account for 45% and 1–5% of severe HA cases, respectively [4]. Inv22 results from non-allelic homologous recombination (NAHR) between the intragenic intron 22 homologous region-1 (*int22h-1*) and two extragenic homologous sequences (*int22h-2* and *int22h-3*) in the Xq28 region [5]. *Int22h-1*, a 9.5 kb sequence within *F8* intron 22, contains *F8A* (OMIM: 305423), the first exon of *F8B* (OMIM: 305424), and their shared bidirectional promoter [6]. *int22h-2* and *int22h-3* show 99.93% mutual identity and are located ~ 488 kb and ~ 566 kb telomeric to *F8*, respectively. These share 99.2% sequence homology with *int22h-1* [6]. Their > 99% sequence homology facilitates NAHR, leading to characteristic *F8* rearrangements including intron 22 inversions, deletions, and duplications. LR−PCR is a widely employed technique for the rapid screening and diagnosis of Inv22 [7]. In this method, primers P and Q are positioned at −1212 bp and + 1334 bp, respectively, flanking the *int22h-1* region, while primers A and B are located at −167 bp and + 118 bp, respectively, flanking the *int22h-2* and *int22h-3*. In normal males, PCR amplification generates two segments: PQ (an amplicon spanning *int22h-1*) and AB (an amplicon spanning *int22h2/h3*). By contrast, in males with severe HA caused by the Inv22, PCR produces three amplicons, including PB (a recombinant amplicon formed by the fusion of primer P targeting *int22h-1* and primer B targeting *int22h2/h3*), AQ (a recombinant amplicon formed by the fusion of primer A targeting *int22h2/h3* and primer Q targeting *int22h-1*), and AB (an amplicon derived from the non-recombined extragenic homolog) [7].

In addition to the typical *F8* Inv22 or Inv1, some studies have reported uncommon *F8* structural rearrangements in severe HA [8–14]. In this study, we investigated the X chromosome structure in a Chinese severe HA pedigree and revealed that a complex genomic rearrangement disrupts the *F8* gene structure, which is attributed to the insertion of duplications in intron 22.

Materials and methods

Subjects

A 2-year-old male presented with severe HA (FVIII:0.2%), initially evaluated at 6 months for prolonged bleeding. Coagulation studies showed markedly prolonged APTT (88.6 s; normal 22.3–32.5 s) with moderately decreased FIX activity (42.7%). Family history identified one affected male in the maternal lineage (great-uncle with confirmed severe HA and disabling arthropathy), while no other family members exhibited abnormal bleeding. The FVIII levels of the patient's other family members were within the normal range. Subsequently, following the detection of abnormal LR-PCR fragment patterns (AQ, PQ, AB) at external institution, the proband was referred to our hospital for molecular diagnosis. Targeted exon capture sequencing of *F8*, performed by a third-party laboratory (Shenzhen BGI Gene Co., China), excluded coding region variants in the proband and his maternal relatives (mother, aunt, grandmother). To confirm the diagnosis and enable prenatal genetic counseling for the proband's maternal aunt, we performed sequential genomic analyses beginning with Affymetrix CytoScan 750 K SNP array and optical genome mapping (OGM) on the proband, followed by OGM confirmation in both the aunt and grandmother to determine inheritance patterns. Oxford Nanopore long-read sequencing (ONT-LRS) was then conducted on the aunt to precisely characterize the structural variant.

Affymetrix CytoScan 750 K SNP array

Peripheral blood (5 mL) was collected from the proband using K2EDTA Vacutainer tubes (Becton Dickinson, USA) to prevent coagulation. Genomic DNA (gDNA) was extracted from the blood samples using a QIAamp DNA Blood Mini Kit (Qiagen, Germany) according to the manufacturer's protocol. The gDNA was then digested, ligated, amplified, purified, fragmented, labeled, hybridized with probes, washed, and scanned via the CytoScan™ 750 K SNP Array (Thermo Fisher Scientific, USA) according to standard operating procedures. A computational analysis of the scanned image results was performed to detect copy number variants using Chromosome Analysis Suite 4.0.

Optical genome mapping

High-molecular-weight (HMW) gDNA was isolated from fresh peripheral blood collected in K2EDTA Vacutainer tubes (Becton Dickinson, USA) from the proband, grandmother, and aunt using the Bionano Prep SP Blood and Cell Culture DNA Isolation Kit (Bionano Genomics, USA) according to the manufacturer's protocol. DNA integrity (> 150 kb) was verified by pulsed-field gel electrophoresis, and quantification was performed using the Qubit dsDNA BR Assay (Thermo Fisher Scientific,

USA). HMW gDNA (750 ng) was fluorescently labeled using DLS DNA Labeling Kit (Bionano Genomics, USA) with DLE-1 enzyme and DL-green fluorophores, followed by counterstaining and quality assessment using a Saphyr system. The labeled DNA molecules were linearized in nanochannel arrays using Saphyr Chips (Bionano Genomics, USA). Raw BNX files were filtered based on a minimum length of 150 Kb and ≥ 9 labeled sites per single molecule. We performed in silico DLE1 digestion of the human reference genome (GRCh38) to generate the reference map, and the preset parameters of the software were used for comparison. The de novo assembly of single molecules to generate consensus genome maps was implemented using Bionano Solve v3.5.1.

Oxford Nanopore long-read sequencing

To obtain high-quality HMW gDNA for ONT-LRS, 5 mL of fresh peripheral blood was collected from the proband's aunt into a K2EDTA Vacutainer tube (Becton Dickinson, USA). High-quality, HMW gDNA was extracted from peripheral blood leukocytes using the manual extraction protocol. The cells were lysed with a lysis buffer, followed by chloroform extraction and isopropanol precipitation. The gDNA was further purified using Agencourt AMPure XP magnetic beads (A63882, Beckman Colter, USA). The integrity of gDNA was assessed by pulsed-field gel electrophoresis (PFGE), confirming high-molecular-weight DNA with optimal integrity. Subsequently, one microgram of gDNA underwent end repair and dA-tailing using the NEBNext® Ultra™ II End Repair/dA-Tailing Module (E7546, New England Biolabs) according to the manufacturer's instructions. The reaction products were purified and eluted using Agencourt AMPure XP beads. Adapter ligation was then performed using the NEBNext Quick Ligation Module (E6056, New England Biolabs) for constructing sequencing libraries. The DNA library was then analyzed via PromethION long-read sequencing (Oxford Nanopore Technologies, UK). The reads were aligned to the human reference genome hg19 using Minimax2 software. structural variations (SVs) analysis was performed using Sniffles software, and RepeatHMM was used for STR analysis. SVs were filtered to retain those with > 2 reads and whose read support after normalization in the 10 kb region upstream and downstream of the variant exceeded the read support after normalization * 0.3 in normal samples. The breakpoint positions were obtained using the SV calling software Sniffles, followed by manual validation in IGV.

Results

The SNP array revealed a 158 kb duplication in the *F8* extragenic region involving exons 2–8 of *TMLHE* genes and the *int22h-3* region (GRCh38: X:155,387,916 – 155,546,034) in the proband, with a resolution of 50 kb (Fig. 1). To increase the resolution of copy number variations (CNVs), OGM was conducted on the proband, his grandmother, and his aunt. OGM achieved an average N50 (> 150 Kb) of 266.25 Kb, a mapping rate of 91.9%, an average label density of 15.44/100 Kb, an effective coverage of 144.74x, and a negative label variance (NLV) of 7.49. In the proband, OGM analysis revealed a 130.3 kb inverted duplication spanning *int22h-2* and a partial *int22h-3* region (GRCh38: X:155,337,184 – 155,467,470), as well as a 91.9 kb direct duplication (GRCh38: X:155,455,366 – 155,547,276) encompassing exons 2–8 of *TMLHE* gene and a partial *int22h-3* region, both located within Xq28 (Fig. 2A). Additionally, OGM marker annotation indicated that duplications were inserted into *F8* intron 22, with the breakpoint at chrX:154,877,228-chrX:154,889,607 (GRCh38) (Fig. 2A). OGM analysis confirmed that the proband's grandmother and aunt carried the identical *F8* rearrangement(Fig. 2B and C), demonstrating maternal inheritance of this structural variant in the proband.

ONT sequencing generated 91.5 Gb of data, with an average read length of 13,529 bp and an average depth of 32x. Through structural variation analysis using Sniffles and validation with IGV, five approximate breakpoints were identified, located at hg19: chrX:154,105,777, 154,113,526, 154,610,638, 154,689,386, and 154,776,950 (Fig. 3A-3D). The int22h family exhibit high sequence similarity but distinguishable by unique single nucleotide variants (SNVs). A chimeric read spanning the critical region demonstrated a rearrangement structure, with its 5' segment (hg19: chrX:154,105,777 – 154,113,526) mapping exclusively to the int22h-1 specific locus, as evidenced by unique SNVs. Conversely, the 3' segment (hg19: chrX:154,113,527 – 154,118,602) aligned with the *int22h-3* specific region. This finding suggests a potential recombination event between *int22h-1* and *int22h-3*(Figure 3B). The ribbon plot illustrates paired-end sequencing reads spanning two duplicated segments (hg19: chrX:154,610,638 – 154,689,386 and chrX:154,689,387 – 154,776,950) in the Xq28 region. Anti-parallel orientation of connecting ribbons indicates a potential inversion-driven recombination event between these duplications (Supplementary Fig. 1). ONT analysis identified three sequential duplications in F8 gene intron 22 (hg19: X:154,105,777), confirmed through integration of breakpoint depth profiles, spanning reads, and genome annotation consistency. These include a 7.75-kb duplication (hg19: X:154,105,777 – 154,113,526) involving a portion of *int22h-1*, a 78.75-kb inverted duplication (hg19: X:154,610,638 – 154,689,386), and an 87.56-kb direct duplication (hg19: X:154,689,387 – 154,776,950) (Fig. 3A-D). Corresponding GRCh38 coordinates are provided in Supplementary Table e1. Reanalysis of the

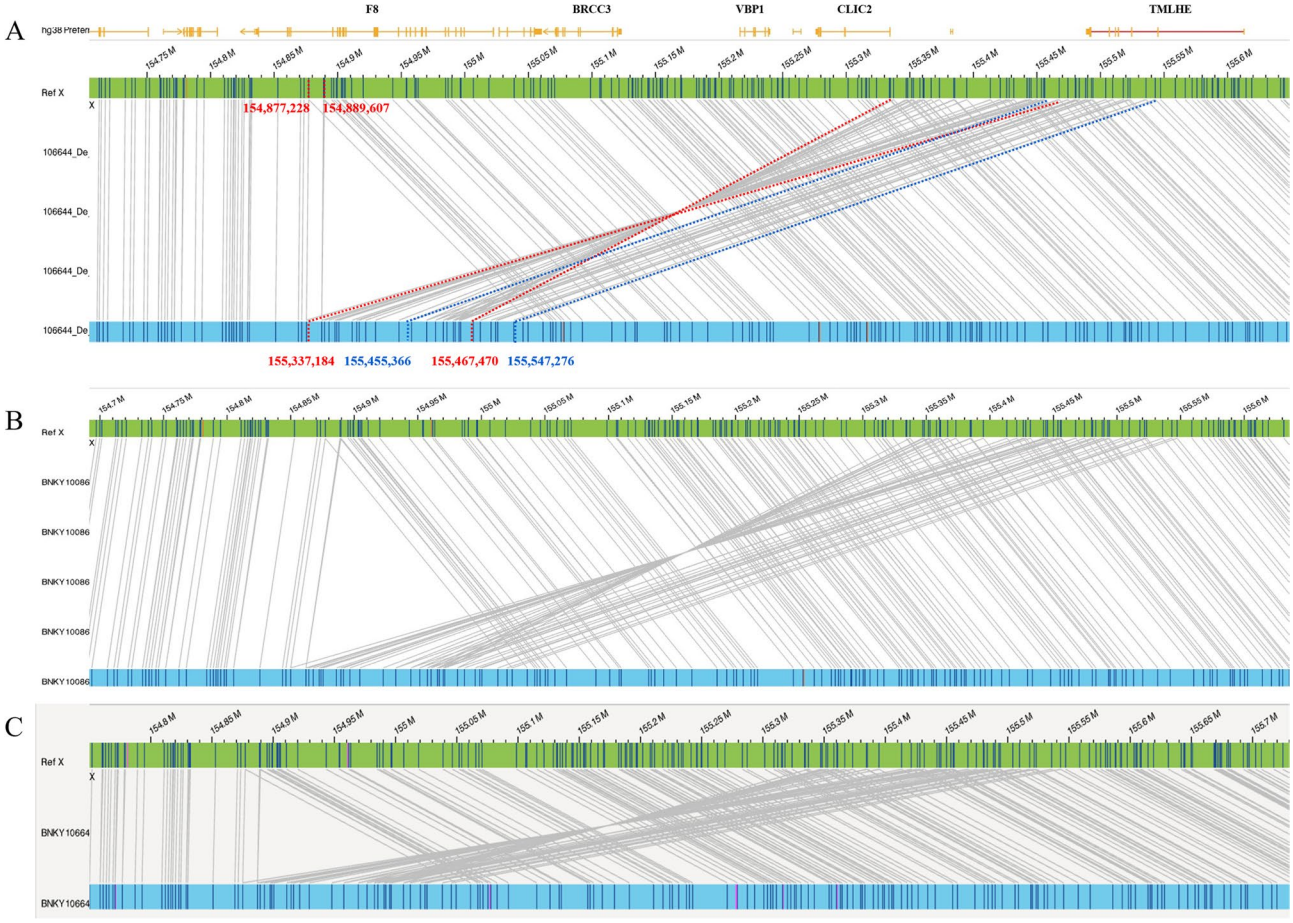

Fig. 1 Duplications at the Xq28 locus detected by Affymetrix CytoScan 750 K assay. The scatter plot depicts copy number variations (CNVs) on Xq28 (GRCh38: X:155,387,916 – 155,546,034) analyzed by weighted log2 ratio, revealing copy number gains (log2 ratio ~ 1) that encompass exons 2–8 of the *TMLHE* gene and the *int22h-3* region. Additionally, an approximately 3 kb signal upshift suggestive of a potential duplication was identified at the breakpoint coordinates X:154,880,715 – 154,883,745 (GRCh38). The solid blue box highlights the duplicated segments in the Xq28 region, while the red dashed box delineated the genomic region spanning *F8* and *TMLHE* genes. Each data point represents either a CNV probe (weighted log2 ratio on the y-axis) or an SNP probe (allele difference on the y-axis), plotted against genomic position (GRCh38: X:148,500,000-155,600,000)

CMA data based on ONT results revealed an upshift in the probe signal within *int22h-1*, corresponding to a 3 kb region (GRCh38: X:154,880,715 – 154,883,745) (Fig. 1).

Although the combined use of ONT-LRS and OGM successfully determined the overall architecture of the *F8* rearrangement, including the size, order, and insertion sites of duplicated/inverted segments, the high sequence homology among *int22h* regions precluded single-nucleotide resolution of breakpoints. Thus, breakpoints were mapped to an approximate location.

Discussion

As of February 2025, the Factor VIII gene (*F8*) variant database (www.factorviii-db.org) has documented 6,211 unique variants, underscoring the extensive genetic diversity of the *F8* gene. Given this complexity, the molecular diagnosis of HA often requires integrating multiple approaches, including LR-PCR, inverse PCR (IS-PCR), short-read high-throughput sequencing (NGS), Sanger sequencing, and multiplex ligation-dependent probe amplification (MLPA) [7, 10, 15]. The initial step employs either LR-PCR or IS-PCR to screen for Inv22 and Inv1in the F8 gene. Subsequent steps utilize NGS to identify single nucleotide variants (SNVs) and MLPA to detect whole-exon deletions and duplications. Notably, Johnsen et al.. demonstrated that NGS-based genotyping can simultaneously detect recurrent inversions, mutations, and CNVs, supporting its potential as a comprehensive diagnostic approach [16].

Conventional molecular diagnostic approaches, including inversion screening, sequencing, and CNV analysis, resolve approximately 99% of severe HA cases. However, in 1–2% of severe HA cases, no F8 abnormality is detected via these methods. Deep intronic variants or rare SVs in the *F8* gene may account for these unresolved cases [17, 18]. In this study, we challenged the accuracy of the initial diagnosis as the proband's LR-PCR results revealed aberrant fragment patterns (AQ, PQ, AB), which

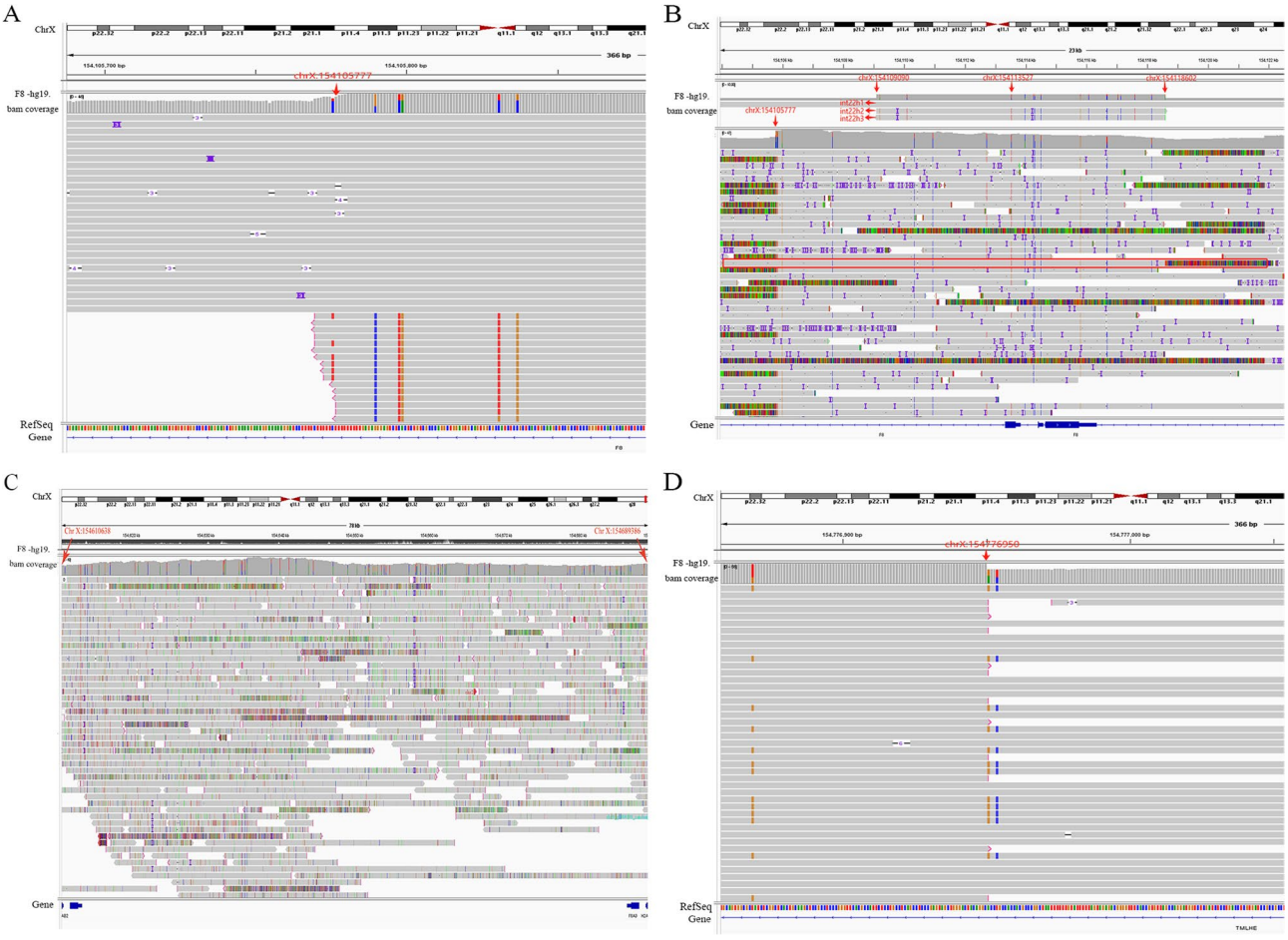

Fig. 2 OGM reveals novel complex structure rearrangements affecting the F8 gene. **A** Optical genome mapping (OGM) analysis of the proband identified two complex structural variants in the Xq28 region: a 130.3 kb inverted duplication (GRCh38: X:155,337,184 – 155,467,470) and a 91.9 kb direct duplication (GRCh38: X:155,455,366 – 155,547,276), both inserted as a contiguous segment into intron22 of the *F8* gene (GRCh38: X:154,877,228 – 154,889,607). **B** and **C**) are the OGM results of the proband's aunt and grandmother, respectively. They carry the same structural variants in the Xq28 region as those identified in the proband, confirming maternal inheritance

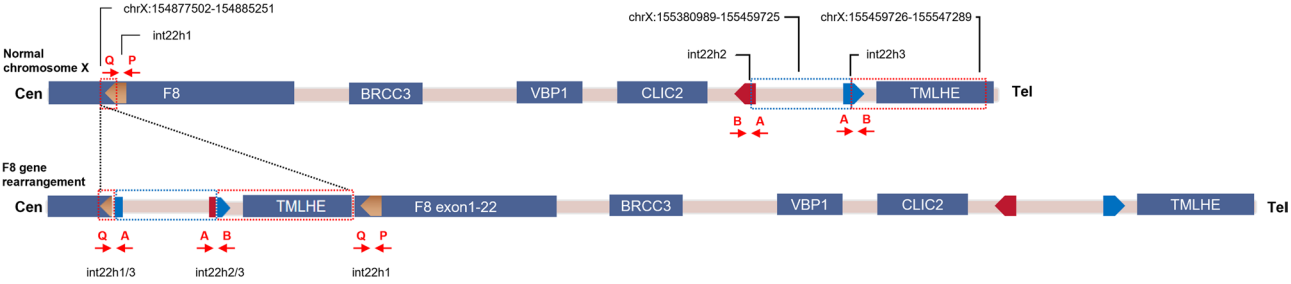

Fig. 3 Chromosomal rearrangement of Xq28 identified via Oxford Nanopore sequencing. Identification of complex structural variants in the Xq28 region using Oxford Nanopore sequencing, including a 7.75 kb duplication sequence (hg19: X:154,105,777 – 154,113,526), a 78.75 kb inverted duplication (hg19: X:154,610,638 – 154,689,386), and an 87.56 kb duplication (hg19: X:154,689,387 – 154,776,950). **A** The Integrated Genomics Viewer (IGV) visualization of split reads supporting the 5′ breakpoint (chrX:154,105,777) of the 7.75 kb duplication. **B** IGV indicated that there may be homologous recombination in the intron 22 and its flanking regions of the F8 gene, with the red box highlighting the suspected homologous recombination between int22h1 and int22h3. **C** IGV coverage plot confirming the 78.75 kb inverted duplication (chrX:154,610,638 – 154,689,386). **D** IGV split-read alignment validating the 3′ breakpoint (chrX:154,776,950) of the 87.56 kb duplication

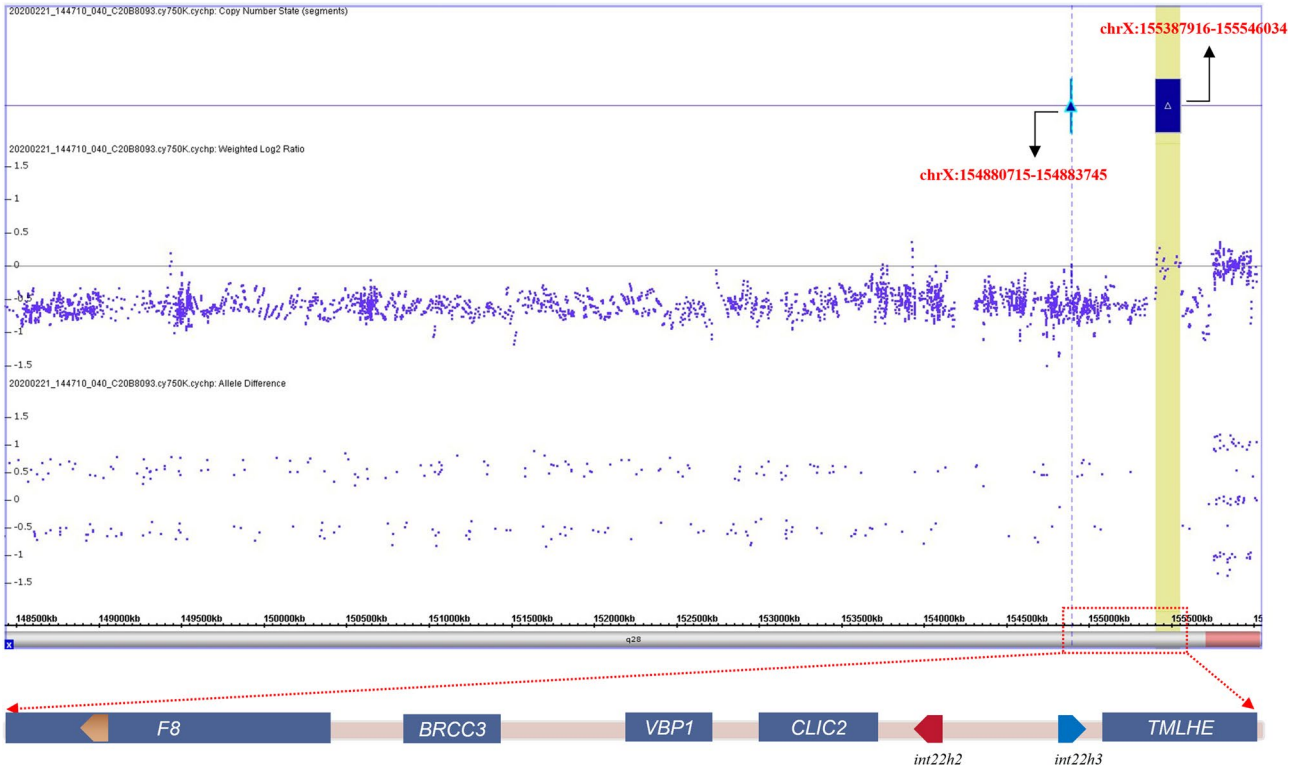

Fig. 4 Schematic description of F8 gene rearrangement Complex F8 rearrangement in the proband's Xq28 region, as resolved by Oxford Nanopore long-read sequencing and optical genome mapping (OGM). The rearrangement comprises three sequentially inserted duplications within *F8* intron 22: a 7.75-kb direct duplication (GRCh38: X:154,877,502 – 154,885,251) containing part of int22h-1, a 78.75-kb inverted duplication (GRCh38: X:155,380,989 – 155,459,725) spanning partial sequences of int22h-3 and int22h-2, and an 87.56-kb direct duplication (GRCh38: X:155,459,726 – 155,547,289) involving part of int22h-3 and exons 2–8 of *TMLHE*. The 78.75 kb inverted duplication connects proximally to the 7.75 kb duplication (int22h1/3 junction, AQ), and distally to the 87.56 kb duplication (int22h2/3, AB). The rearrangement retain the complete *int22h-1* (PQ), *int22h-2*, and *int22h-3* (AB) regions. P, Q, A, and B indicate the binding sites of the primers used for long-range PCR to detect int22h-related inversions

was inconsistent with the expected results for HA. ONT analysis revealed a complex rearrangement involving int22h-mediated duplications in the *F8* gene, which was consistent with the aberrant fragment patterns observed by LR-PCR. Homologous recombination between a partial duplication of *int22h-1* (within the 7.75 kb direct duplication) and a partial duplication of *int22h-3* (within the 78.75 kb inverted duplication) generated the *int22h1-int22h3* junction (AQ).The native *int22h-1* (PQ), *int22h-2*, and *int22h-3* (AB) regions remain largely intact in their original genomic contexts, while the rearranged locus contains duplicated and inverted segments derived from these homologous regions (Fig. 4).

Chromosomal inversions typically do not result in a net gain or loss of genomic material. However, rare non-canonical rearrangements involving deletions or duplications of *int22h* and other genes have been reported, which are often classified as aberrant or abnormal patterns of Inv22 [12, 13]. Duplications including the *int22h-2* and i*nt22h-3* regions, have also been recorded in the Database of Gnom AD SV V4.1 in healthy individuals. Lannoy N et al.. proposed that duplications of *int22h-2* and *int22h-3* frequently recombine with each other, suggesting that these events may represent structural variation polymorphisms [5]. In this study, an 158 kb duplication involving *int22h-3* and exons 2–8 of the *TMLHE* gene, detected via SNP array, could be classified as a polymorphic variation according to the American College of Medical Genetics and Genomics (ACMG) and the Clinical Genome Resource (ClinGen) guidelines. However, the clinical significance of int22h duplications depends on their alignment, position, and underlying mechanisms [5]. While the SNP array identified a duplication in the *F8* extragenic region, it could not determine orientation and functional impact of the duplication.

As a next-generation cytogenetic technology with a resolution of approximately 500 bp, OGM is capable of identifying chromosomal abnormalities, including CNVs, balanced rearrangements, and repeat amplifications [19]. Previous studies have confirmed that OGM is highly consistent with karyotyping and CMA in detecting CNVs and SVs [19, 20]. Moreover, OGM offers distinct advantages in identifying clinically significant cryptic balanced translocations and complex chromosomal rearrangements [8, 21]. Fahiminiya S et al.. demonstrated that OGM is an effective diagnostic tool for detecting both

known recurrent inversions in *F8* and novel complex Inv22 events accompanied by *F8* extragenic duplications [9]. In this study, OGM identified the *F8* complex rearrangements involving highly homologous int22h regions in HA proband, demonstrating its utility for characterizing such SVs.

To resolve ambiguities in breakpoint assignment across int22h homologs and determine the topological relationship between the duplications, we conducted ONT sequencing, we conducted ONT sequencing on the proband's aunt. ONT-LRS is particularly useful for analyzing large SVs and complex genomic regions, which are challenging to resolve with short-read NGS. Previous studies have reported the use of LR–PCR and LRS-based assays to identify *F8* variants, significantly improving the genetic diagnosis of HA. However, these methods may miss large duplications or deletions not covered by the primers [18, 22]. In this study, we employed ONT-LRS to validate the complex SVs in the *F8* gene involving *int22h* regions, ensuring the accuracy of the OGM findings. ONT confirmed that an inverted duplication and a direct duplication were sequentially inserted into *F8* gene intron 22. Owing to the 500 bp resolution limit of OGM, ONT further identified an additional 7.75 kb duplication, including a partial duplication of *int22h-1*. We hypothesize that the insertion of these duplications into intron 22 of the *F8* gene disrupts its expression, leading to severe HA in this pedigree. ONT was also proven to be an efficient strategy for the identification of *F8* complex recombination mediated by int22h regions in HA patient.

Through the combined application of OGM and ONT technologies, we have revealed the *F8* complex recombination event involving five critical breakpoints in Xq28 region. Among these, three breakpoints mapped to the highly homologous int22h regions, while the remaining two were localized to distinct genomic loci: one within exons 2–8 of the *TMLHE* gene (GRCh38: X:155,547,289) and another in the distal portion of *F8* intron 22 (GRCh38: X:154,877,502). Due to the extreme sequence homology of the int22h regions, ONT-LRS alignment encountered multi-mapping phenomena, preventing precise determination of which homologous copy contained the breakpoints. By employing flanking sequence anchoring and read depth analysis, we were able to indirectly localize the breakpoint positions. Concurrently, OGM provided independent, high-resolution genomic physical maps through label pattern analysis, identifying a 130.3 kb inverted duplication and a 91.9 kb direct duplication in the Xq28 region. Through integrative analysis of ONT and OGM datasets, we successfully resolved the macro-scale topological architecture of the recombination event. However, single-nucleotide resolution of the breakpoints could not be achieved.

In conclusion, the complex recombination mediated by int22h regions duplications in this pedigree disrupts *F8* expression, resulting in severe HA in proband. OGM and ONT have significantly increased our ability to identify *F8* complex genomic rearrangements, particularly in cases unresolved by conventional genetic approaches. The *F8* complex structural variants identified in this study represent a novel rearrangement pattern that, to our knowledge, has not been previously reported in the literature, thereby expanding the spectrum of genetic alterations associated with severe HA. While our study successfully characterized the macroscopic architecture of this complex rearrangement, the precise molecular mechanisms underlying the recombination events remained unresolved due to the inability to achieve single-nucleotide resolution of breakpoints within the highly homologous *int22h* regions. To address this limitation, future studies could employ targeted long-range PCR amplification spanning predicted breakpoint junctions, followed by TA cloning and high-throughput Sanger sequencing of multiple clones. This approach would enable precise nucleotide-level mapping of breakpoints and reveal the rearrangement mechanism.

Supplementary Information

The online version contains supplementary material available at https://doi.org/10.1186/s12920-025-02202-8.

Supplementary Material 1.

Supplementary Material 2.

Acknowledgements

The authors thank the family members for their cooperation in this study.

Authors' contributions

YZ and YM drafted the manuscript and designed the experiments. LY collected the patient's information. CH and JX conducted the experiments. JG, BL and BX analysed and interpreted the Datas. CC provided funding. SW recruited the patient and follow-up. HL reviewed the manuscript and provided funding.

Funding

This work was supported by grants from the Ningbo Science and Technology Project (No. 2023Z178), the Key Technology Breakthrough Program of Ningbo Sci-Tech Innovation YONGJIANG 2035 (No. 2024Z221), the Ningbo Healthcare high-end team project (2022020405), and the Medical and Health Science and Technology Program of Zhejiang Province (2025KY1426).

Data availability

Details of the variants analyzed in this study have been deposited in the ClinVar database (https://www.ncbi.nlm.nih.gov/clinvar/), with accession numbers VCV003366903.1, VCV003366902.1 and VCV003366901.1.

Declarations

Ethics approval and consent to participate

In accordance with the Declaration of Helsinki, all of the participants and parents of the minors provided informed consent to participate in the study. This study was approved by the IRB of The Affiliated Women and Children's Hospital of Ningbo University (No. EC2020-048).

Consent for publication
All the participants and the parents of minors gave written informed consent for their personal or clinical details along with any identifying images, to be published in this study.

Competing interests
The authors declare no competing interests.

Author details
[1]The Central Laboratory of Birth Defects Prevention and Control, The Affiliated Women and Children's Hospital of Ningbo University, Ningbo, China
[2]Ningbo Key Laboratory for the Prevention and Treatment of Embryogenic Diseases, The Affiliated Women and Children's Hospital of Ningbo University, Ningbo, China
[3]Ningbo Key Laboratory of Genomic Medicine and Birth Defects Prevention, The Affiliated Women and Children's Hospital of Ningbo University, Ningbo, China
[4]Public Health Department, The Affiliated Women and Children's Hospital of Ningbo University, Ningbo, China
[5]Advanced Institute of Information Technology, Peking University, Beijing, China
[6]Grandomics Biosciences, Beijing, China
[7]The Central Laboratory of Birth Defects Prevention and Control, Ningbo Key Laboratory of Genomic Medicine and Birth Defects Prevention, The Affiliated Women and Children's Hospital of Ningbo University, 339 Liuting Street, Haishu District, Ningbo, Ningbo 315012, China
[8]Ningbo Key Laboratory of Genomic Medicine and Birth Defects Prevention, The Affiliated Women and Children's Hospital of Ningbo University, 339 Liuting Street, Haishu District, Ningbo 315012, Zhejiang, China

Received: 5 March 2025 / Accepted: 28 July 2025
Published online: 27 August 2025

References

1. Oldenburg J, Ananyeva NM, Saenko EL. Molecular basis of haemophilia A. Haemophilia. 2004;10(Suppl 4):133–9.
2. White GN, Rosendaal F, Aledort LM, Lusher JM, Rothschild C, Ingerslev J. Definitions in hemophilia. Recommendation of the scientific subcommittee on factor VIII and factor IX of the scientific and standardization committee of the international society on thrombosis and haemostasis. Thromb Haemost. 2001;85(3):560.
3. Gitschier J, Wood WI, Goralka TM, Wion KL, Chen EY, Eaton DH, Vehar GA, Capon DJ, Lawn RM. Characterization of the human factor VIII gene. Nature. 1984;312(5992):326–30.
4. Lannoy N, Hermans C. Review of molecular mechanisms at distal Xq28 leading to balanced or unbalanced genomic rearrangements and their phenotypic impacts on hemophilia. Haemophilia. 2018;24(5):711–9.
5. Lakich D, Kazazian HJ, Antonarakis SE, Gitschier J. Inversions disrupting the factor VIII gene are a common cause of severe haemophilia A. Nat Genet. 1993;5(3):236–41.
6. Lannoy N, Hermans C. Principles of genetic variations and molecular diseases: applications in hemophilia A. Crit Rev Oncol Hematol. 2016;104:1–8.
7. Liu Q, Nozari G, Sommer SS. Single-tube polymerase chain reaction for rapid diagnosis of the inversion hotspot of mutation in hemophilia A. Blood. 1998;92(4):1458–9.
8. Qu J, Li S, Yu D. Detection of complex chromosome rearrangements using optical genome mapping. Gene. 2023;884:147688.
9. Fahiminiya S, Oikonomopoulos S, Rivard GE, Gandhi M, Scott P, Montpetit A, Chen SH, Park K, Vezina C, Ragoussis J, et al. Deciphering a novel complex inversion affecting F8 in a family with severe haemophilia A by optical genome mapping. Haemophilia. 2023;29(3):921–4.
10. Wang X, Wang H, Tan H, Liu XP, Li H. An aberrant F8 intron 1 inversion with concomitant large duplication and deletion in a Chinese severe hemophilia A patient. HEMATOLOGY. 2021;26(1):53–7.
11. Tokoro M, Tamura S, Suzuki N, Kakihara M, Hattori Y, Odaira K, Suzuki S, Takagi A, Katsumi A, Hayakawa F, et al. Aberrant X chromosomal rearrangement through multi-step template switching during sister chromatid formation in a patient with severe hemophilia A. Mol Genet Genomic Med. 2020;8(9):e1390.
12. Jourdy Y, Chatron N, Fretigny M, Carage ML, Chambost H, Claeyssens-Donadel S, Roussel-Robert V, Negrier C, Sanlaville D, Vinciguerra C. Molecular cytogenetic characterization of five F8 complex rearrangements: utility for haemophilia A genetic counselling. Haemophilia. 2017;23(4):e316-23.
13. Chen C, Xie X, Wu X, Lu Y, Wang X, Wu W, Hu Y, Ding Q. Complex recombination with deletion in the F8 and duplication in the TMLHE mediated by int22h copies during early embryogenesis. Thromb Haemost. 2017;117(8):1478–85.
14. You G, Chi K, Lu Y, Ding Q, Dai J, Xi X, Wang H, Wang X. Identification and characterisation of a novel aberrant pattern of intron 1 inversion with concomitant large insertion and deletion within the F8 gene. Thromb Haemost. 2014;112(2):264–70.
15. Zhang X, Chen K, Bian S, Wang G, Qin X, Zhang R, Yang L. Molecular diagnosis of hemophilia A and pathogenesis of novel F8 variants in Shanxi, China. Glob Med Genet. 2023;10(3):247–62.
16. Johnsen JM, Fletcher SN, Huston H, Roberge S, Martin BK, Kircher M, Josephson NC, Shendure J, Ruuska S, Koerper MA, et al. Novel approach to genetic analysis and results in 3000 hemophilia patients enrolled in the my life, our future initiative. Blood Adv. 2017;1(13):824–34.
17. Bagnall RD, Waseem NH, Green PM, Colvin B, Lee C, Giannelli F. Creation of a novel donor splice site in intron 1 of the factor VIII gene leads to activation of a 191 bp cryptic exon in two haemophilia A patients. Br J Haematol. 1999;107(4):766–71.
18. Chatron N, Schluth-Bolard C, Fretigny M, Labalme A, Vilchez G, Castet SM, Negrier C, Sanlaville D, Vinciguerra C, Jourdy Y. Severe hemophilia A caused by an unbalanced chromosomal rearrangement identified using nanopore sequencing. J THROMB HAEMOST. 2019;17(7):1097–103.
19. Xie M, Zheng ZJ, Zhou Y, Zhang YX, Li Q, Tian LY, Cao J, Xu YT, Ren J, Yu Q, et al. Prospective investigation of optical genome mapping for prenatal genetic diagnosis. CLIN CHEM. 2024;70(6):820–9.
20. Sahajpal NS, Barseghyan H, Kolhe R, Hastie A, Chaubey A. Optical genome mapping as a Next-Generation cytogenomic tool for detection of structural and copy number variations for prenatal genomic analyses. Genes (Basel). 2021;12(3):398.
21. Yang H, Garcia-Manero G, Sasaki K, Montalban-Bravo G, Tang Z, Wei Y, Kadia T, Chien K, Rush D, Nguyen H, et al. High-resolution structural variant profiling of myelodysplastic syndromes by optical genome mapping uncovers cryptic aberrations of prognostic and therapeutic significance. Leukemia. 2022;36(9):2306–16.
22. Liu Y, Li D, Yu D, Liang Q, Chen G, Li F, Gao L, Li Z, Xie T, Wu L, et al. Comprehensive analysis of hemophilia A (CAHEA): towards full characterization of the F8 gene variants by long-read sequencing. Thromb Haemost. 2023;123(12):1151–64.

Publisher's Note